

Near-infrared OPO in an AlGaAs/AlOx waveguide

C. Ozanam^a, M. Savanier^a, L. Lanco^b, X. Lafosse^b, A. Andronico^a, I. Favero^a, S. Ducci^a, G. Leo^{*a}

^aUniversité Paris Diderot, Sorbonne Paris Cité, Laboratoire Matériaux et Phénomènes Quantiques, CNRS-UMR 7162, Case courrier 7021, 75205 Paris Cedex 13, France; ^bLaboratoire de Photonique et Nanostructures, CNRS-UPR20, Route de Nozay, 91460 Marcoussis, France.

ABSTRACT

Within the ambitious quest for an electrically pumped version of the optical parametric oscillator (OPO), we demonstrate the first near-infrared integrated OPO in a direct gap semiconductor. This nonlinear device is based on a selectively oxidized GaAs/AlAs heterostructure, the same “AlOx” technology that is at the heart of VCSEL fabrication. The heterostructure and waveguide design allows for type-I form-birefringent phase matching, with a TM₀₀ pump around 1 μm and TE₀₀ signal and idler around 2 μm. Relying on the high non-resonant $\chi^{(2)}$ of GaAs, relatively weak guided-wave optical losses, and monolithic SiO₂/TiO₂ dichroic Bragg mirrors, we observe a threshold of 210 mW at degeneracy in the continuous-wave regime, with a single-pass-pump doubly resonant scheme. Further improvement can be achieved by adopting a double-pump-pass scheme and, in a more fundamental way, by further optimizing the waveguide optical losses. The latter are induced by a not entirely mastered AlAs oxidation process and are of two distinct types: Rayleigh-like scattering at signal and idler wavelength ($\alpha \leq 1\text{cm}^{-1}$), due to the interface roughness between GaAs and AlOx layers; and absorption at pump wavelengths ($\alpha \approx 3\text{cm}^{-1}$), due to volume defects in the GaAs layers adjacent to the aluminum oxide. This result marks a milestone for integrated nonlinear photonics and represents a significant step toward the goal of a broadly tunable coherent light source on chip.

Keywords: optical parametric oscillator, waveguide, AlOx, nonlinear optics, form birefringence, semiconductor.

1. INTRODUCTION

The optical parametric oscillator (OPO), one of today’s most known optical devices, can be functionally defined as a widely tunable coherent source [1]. Like the laser, it is based on the resonant feedback provided by a cavity to an optical amplifier, but it relies on parametric amplification rather than stimulated emission. Unlike the laser, whose heterostructure diode version [2] has propelled the field of photonics, the quest for an electrically pumped monolithic version of the OPO is still open half a century after its original demonstration [3]. While most of guided-wave OPOs have been demonstrated in LiNbO₃ [4-6], its dielectric nature is incompatible with the perspective of full optoelectronic integration, which seems more viable for a direct gap semiconductor with strong nonlinearity.

In this context, a major breakthrough would be the demonstration of an electrically pumped OPO integrated on a chip, which could be used as a coherent variable wavelength emitter in spectral ranges where semiconductor lasers are only poorly tunable. The potential impact of a monolithic OPO is apparent if we compare the wavelength tunability $\Delta\lambda$ of an integrated InGaAsP SG-DBR single-mode telecom laser diode ($\Delta\lambda \approx 60$ nm for a control current change of 90 mA [7]) and a guided-wave OPO based on periodically poled LiNbO₃ ($\Delta\lambda \approx 900$ nm for a pump tuning of 16 nm [6])

Let us stress that the perspective of the full convergence at chip-scale level between optics and electronics has been a major driving force for scientific and technological efforts in photonics for the last decades. Of course a large number of applications might benefit from the merging of coherent light sources and the technologically advanced silicon platform [8]. However, the perspective of monolithic silicon photonics is limited by its indirect gap and centrosymmetric crystal

* giuseppe.leo@univ-paris-diderot.fr; phone +33 1 572-76227; fax +33 1 572-76241; mpq.univ-paris-diderot.fr

structure, with the related lack of electrically injected lasers and second-order nonlinear optical components. This explains the interest drawn by AlGaAs waveguides, which stems from the numerous advantages of this III-V direct-gap semiconductor, well known as an established laser material: high second-order susceptibility ($d_{14} \approx 100$ pm/V), wide transparency window (from 0.9 to 17 μm), good thermal conductivity and mature technology.

Here we demonstrate a near-IR continuous-wave (CW) OPO in a form-birefringent GaAs/AlGaAs waveguide, with a low pump threshold $P_{\text{th}} = 210$ mW. The development of such a source might radically transform a number of applications in near and mid IR up to 3 μm . Besides two telecom windows of paramount importance (around 1.3 and 1.5 μm), this spectral region contains the roto-vibrational lines of many relevant molecules (pollutants, toxins, etc.), which makes it essential for civilian and military applications such as spectroscopy, material processing, molecular sensing, thermal imaging, and defense.

Because of the key role played by phase matching (PM) in parametric interactions, let us recall that the optical isotropy of GaAs deprives this cubic material of the standard option of birefringent PM, and it has prompted several alternative approaches for fulfilling this condition [9]. To date, the main PM strategies that have been investigated in the near-IR for guided-wave nonlinear interactions in GaAs are quasi-PM [10], modal PM [11,12] and form-birefringence PM [13], but none of them has resulted yet in an integrated OPO. In the last years orientation-patterned GaAs in the mid-IR has undergone constant progress with high-power OPOs exhibiting thresholds of ≈ 2 kW in the pulsed regime and ≈ 7 W in the CW regime [14,15]. However, the transposability of this approach to a near-IR integrated platform seems to be hindered by large scattering losses at short wavelengths, and by the lack of GaAs-based high-power pump lasers around 2 μm . Therefore the route to a fully integrated tunable semiconductor source of near-IR light remains open and challenging.

The rest of this paper is organized as follows: Section 2 is devoted to the form-birefringence PM technology in AlGaAs waveguides, including the study of the optical propagation losses; the design, the fabrication and the characterization of integrated mirrors are addressed in Section 3; the experimental demonstration of the OPO is provided in Section 4, along with the discussion; conclusions and perspectives are drawn in Section 5.

2. FORM BIREFRINGENT PHASE MATCHING IN AlGaAs WAVEGUIDES

In order to artificially induce a significant amount of birefringence between the fundamental TE_{00} and TM_{00} modes of a waveguide that is fabricated with an isotropic material, one can pattern its core at sub-wavelength scale, by repeatedly breaking the refractive index continuity with a two-materials multilayer. The resulting metamaterial behaves as a macroscopic uniaxial crystal, whose birefringence is fully determined by the index contrast and the filling factors of the materials [16]. In the AlGaAs platform, the form-birefringence-PM approach has been developed during the late 90's at Thomson CSF Laboratory (today III-V Lab) [13].

Actually the first phase-matched interaction of this type had been demonstrated back in the seventies, with the doubling of a CO_2 laser emitting at 10.6 μm [17]. In that case, given the weak material dispersion in the mid-infrared range (few 10^{-2}) an AlAs/GaAs heterostructure suffices to meet the PM condition. However, since the material dispersion strongly increases when the frequencies of the interacting waves lie close to the band gap of the material, nonlinear interactions between the visible and the mid-infrared are prevented for the simple AlGaAs platform.

In 1990, the discovery of selective wet oxidation of Al-rich AlGaAs layers drastically broadened the potential of form-birefringent PM, thanks to the density, homogeneity and stability of a new type of aluminum oxide [18]. This material exhibits nice optical properties, such as a wide transparency window and a low refractive index of ~ 1.6 , and is electrically insulating. A few engineering domains rapidly took advantage of these physical properties: electronics, with field effect transistors [19]; optics, with broadband Bragg mirrors [20]; and optoelectronics, by combining optical and electrical confinement in vertical-cavity surface-emitting lasers (VCSELs) to improve their yield and ensure single-mode emission [21].

In the case dealt with here, the GaAs/ AlOx system allows accessing a birefringence of several 10^{-1} , i.e. up to one order of magnitude higher than in a GaAs/AlAs heterostructure. This in turn enables to phase-match any nonlinear quadratic interaction with wavelengths spanning from the visible to the mid-IR region [22,23].

The structure that we consider here has been designed to operate as an OPO in the near IR, with degeneracy at 1.064 μm . It relies on a guided-wave type-I FBPM scheme between a TM_{00} pump mode at wavelength λ_p and two TE_{00} signal/idler

modes at wavelengths λ_s and λ_t , respectively. The corresponding vertical layout, depicted in Fig. 1a along with the interacting mode profiles, consists of GaAs (substrate) / 1 μm $\text{Al}_{0.92}\text{Ga}_{0.08}\text{As}$ (spacer) / 1 μm $\text{Al}_{0.7}\text{Ga}_{0.3}\text{As}$ (bottom cladding) / $4 \times [37.5 \text{ nm } \text{Al}_{0.98}\text{Ga}_{0.02}\text{As} / 273 \text{ nm } \text{GaAs}] / 37.5 \text{ nm } \text{Al}_{0.98}\text{Ga}_{0.02}\text{As}$ (core) / 1 μm $\text{Al}_{0.7}\text{Ga}_{0.3}\text{As}$ (top cladding) / 30 nm GaAs (protective cap).

This heterostructure has been grown by molecular beam epitaxy on a semi-insulating (001) GaAs substrate. Guiding ridges have been defined along the crystalline axis by means of UV photolithography, then chemically etched with a $\text{CH}_3\text{COOH}:\text{HBr}:\text{K}_2\text{Cr}_2\text{O}_7$ solution, resulting in waveguides with extremely smooth sidewalls, as it can be appreciated from the SEM picture given in Fig. 1b. Typical waveguides are 3 to 4 μm wide, $\sim 3 \mu\text{m}$ deep and cleaved with a length $L = 3 \text{ mm}$. Eventually, $\text{Al}_{0.98}\text{Ga}_{0.02}\text{As}$ has been selectively transformed into AlOx by thermal wet oxidation. This process is performed in a tubular quartz oven at a temperature between 400 and 450°C, exposing the waveguide sidewalls to an oxidizing gas stream [24]. In our setup, the latter is obtained by flowing dry N_2 (2L/min) through a water-filled bubbler heated at 70°C.

Optical propagation losses play a key role in all guided-wave phase-matching schemes, and their reduction is a critical issue. For this purpose, we optimized the thermal wet oxidation process using the feedback provided by systematic loss measurements. In addition, we investigated the possible loss mechanisms in order to single out specific technological limitations and initiate an adequate technological development.

After careful calibration of the oxidation apparatus, we confirmed that 1) the average loss level suffers from slow oxidation kinetics (i.e. from low temperature, since the reaction is thermally activated), and 2) the process must be stopped at the exact moment when the oxidation fronts merge at the center of the structure (i.e. when all the $\text{Al}_{0.98}\text{Ga}_{0.02}\text{As}$ has been converted into AlOx). In our case, the sample has been oxidized at 420°C for 14 minutes, which is our best trade-off between speed and reproducibility.

Despite this care, the present level of optical losses in such AlGaAs/ AlOx waveguides is still significant: $\alpha \sim 0.7$ to 1.5 cm^{-1} around $\lambda = 1.55 \mu\text{m}$. As a comparison, typical PPLN waveguide losses are in the range of few 0.01 cm^{-1} , enabling the fabrication of several cm-long OPOs with threshold as low as $\sim 10 \text{ mW}$ [25]. Thus, in order to develop a low-loss AlGaAs/ AlOx waveguide technology, a better understanding of the optical loss mechanisms involved in such selectively oxidized AlGaAs devices is crucial.

Most of the propagation losses clearly originate from the oxidation process, for they are about three times lower before oxidation (~ 0.1 to 0.5 cm^{-1} around $\lambda = 1.55 \mu\text{m}$). However, the relevant loss mechanisms and their link with the AlOx properties remain uncertain. In particular, several aspects of the oxidation process are not yet clearly established, including the exact formation reactions and the fine chemical and structural properties of the oxide.

The characterization of oxidized layers via transmission electron microscopy (TEM) [26], which was carried out to assess the chemical and morphological properties of AlOx at microscopic scale, has established that:

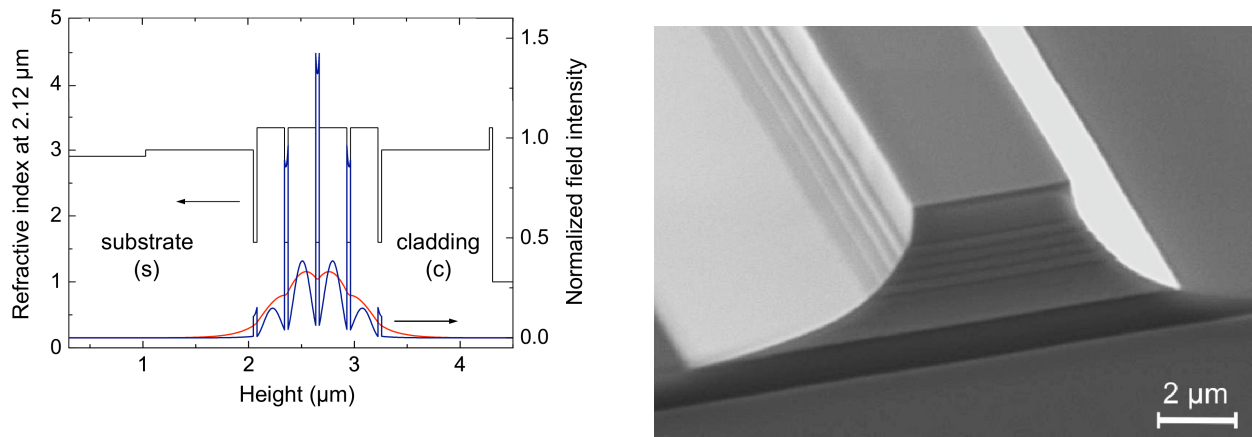


Figure 1. Left: Vertical index profile (thin solid line) and simulated phase-matched interacting modes at $\lambda_p = 1.064 \mu\text{m}$ (solid blue line) and $\lambda_s = \lambda_t = 2.128 \mu\text{m}$ (dotted red line), Right: SEM picture of a waveguide cleaved facet after oxidation.

- AlOx layers are composed of γ -Al₂O₃ polycrystalline grains, sized between 10 and 20 nm, embedded in an amorphous Al_xO_y matrix,
- The roughness at AlGaAs/AlOx interfaces is increased by about 40% and 80% for GaAs and Al_{0.7}Ga_{0.3}As respectively,
- Residual oxidation of the neighboring GaAs and Al_{0.7}Ga_{0.3}As layers occurs through the interfaces over 3 and 9 nm respectively,
- Further in the GaAs layers surrounding the AlOx, the material becomes amorphous in the vicinity of the oxidized layers (~20 nm from the interface) and remains mono-crystalline beyond.

For high-index-contrast waveguides, optical losses are very sensitive to imperfections. We recall that the device dealt with here is passive, thus the semiconductor alloys have been chosen to be transparent at all the wavelengths involved in the $\chi^{(2)}$ process. In addition, in these waveguides operating in CW with internal pump powers $P_p \leq 250$ mW, the contribution of two-photon absorption is not significant as α_{TPA} is ≤ 0.2 cm⁻¹. Hence, assuming a good confinement, i.e. no optical leakage in the substrate by design, losses can only arise from scattering by rough interfaces or volume inhomogeneity, or from absorption by point defects.

Based on the above observations, our starting hypothesis was to ascribe the guided modes propagation losses to scattering. However, the index contrast between AlOx and γ -Al₂O₃ being negligible, polycrystalline grains are not expected to contribute significantly to losses, thus we focused on the roughness of the (Al)GaAs/AlOx boundaries.

Among the different existing techniques to evaluate optical propagation losses, we opted for the Fabry-Perot fringes method [27], which is well suited for $\alpha \leq 1$ cm⁻¹ and only requires the knowledge of the modal reflectivity (estimated by 3D-FDTD simulations). However, for losses of several cm⁻¹, this technique is less reliable and we switched to transmission measurements. Let us recall that, unlike the Fabry-Perot technique, the accuracy of the latter also depends on the estimations of the coupling and collection efficiencies, which are calculated indirectly.

We measured the losses of the TM₀₀ mode (resp. TE₀₀) around 1.064 μ m (resp. 2.128 μ m). Around the degeneracy of parametric fluorescence, when the wavelength of the TM₀₀ pump mode is tuned from 950 and 1060 nm, the TE₀₀ signal wavelength ranges from 1060 nm to 2120 nm. Accordingly, we used a set of linearly polarized CW lasers, tunable between 1280 – 1610 nm (Tunics telecom external cavity diode lasers), and around 2120 nm (Nanoplus DFB laser diode) for the Fabry-Perot fringe measurements, and between 950 – 1100 nm (Spectra-Physics Ti:Sapphire laser) for the transmission measurements.

The experimental results are given in Fig. 2, where it appears that the error bars for the pump-mode data are significantly bigger than their signal-idler counterparts. As mentioned above, the transmission method is indeed less reliable than the Fabry-Perot one, so that the uncertainty is increased. Compared to the data acquired in the telecom band, also the data at 2.12 μ m lack reliability and overestimate the actual loss value. This is due to the limited tunability of the laser diode ($\Delta\lambda \sim 1$ nm) used for this measurement, which does not allow us to refine this estimate based on the Fabry-Perot method.

Two different regimes can be clearly distinguished in Fig. 2:

- Above $\lambda \sim 1.1$ μ m, losses are of the order of 1 cm⁻¹ and decay as an inverse power law of the wavelength $\alpha \propto \lambda^{-N}$. According to the fits of the upper and lower bounds of the prediction band, we find $1.9 \leq N \leq 2.5$. The fair agreement between the experimental data and the model prediction confirms that in this spectral region, losses originate from scattering due to the AlOx layers rough interfaces.
- Below $\lambda \sim 1.1$ μ m, losses are much higher (up to 3 cm⁻¹) and diverge when λ decreases, as highlighted by the phenomenological exponential fit $\alpha \propto \exp[-\lambda/141]$, which clearly deviates from the prediction band.

Very little literature addresses directly the study of optical losses in AlGaAs/AlOx devices beyond 1 μ m. In particular, for $\lambda < 1.1$ μ m, the sole scattering on surface imperfections is not sufficient to explain the propagation loss behavior, and a new loss mechanism, most likely accounting for bulk defects in the vicinity of the oxide layers, had to be considered. While the high level of losses and their exponential decay with wavelength shown in Fig. 2 are reminiscent of Urbach's tail absorption model, the origin of this absorption is still unclear at the moment. Since Al₂O₃ and GaAs themselves are known to be transparent in the near IR, we tentatively ascribe these additional losses to point defects associated to energy levels in the semiconductor gap and created during the oxidation process in the GaAs layers adjacent to AlOx. Arsenic antisites (As_{Ga}) have already been supposed to introduce donor levels with similar properties in the gap of AlGaAs, in

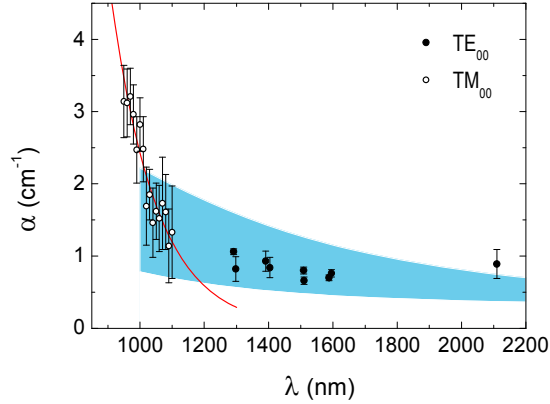


Figure 2. Propagation losses of the fundamental TM (circles) and TE (dots) modes vs. wavelength λ . Below $\lambda \sim 1.1 \mu\text{m}$, data are fitted by the decaying exponential $\exp[-\lambda/141]$ (red solid line). Above $\lambda \sim 1.1 \mu\text{m}$, the experimental data are bounded by the simulation results (blue stripe).

optical devices [28] as well as in electrical devices [29]. Such defects might arise from trapped oxidation reaction products resulting in an excess of elemental arsenic As^0 at the oxide-semiconductor interfaces. Many As_{Ga} would then be generated after the diffusion of As^0 into the neighboring semiconductor layers [30], consistently with the TEM observations recalled above [26].

Since propagation losses are currently the limiting factor for the demonstration of efficient integrated AlGaAs/AIOx devices, further minimization remains to be tackled. To this purpose four potential solutions are under study:

- Based on existing research on quantum-well luminescence close to oxidized layers, hydrogenation might be tried in order to remove absorbing species trapped at the oxide interfaces [31],
- Thermal annealing is also expected to diffuse defects out of the structure, and to restore the crystallinity of the amorphous materials,
- Shifting the coalescence of the counter-propagative oxidation fronts away from the center of the waveguide (i.e. where the fields are maximums) should prevent the formation of additional defects induced by over oxidation [32].
- The insertion of thin lattice-matched GaInP barriers between the AlOx and GaAs layers seems effective to hamper the diffusion of As-rich oxidation reaction products into the latter, thus preventing the formation of point defects [33].

We can conclude this section by resuming that, despite the recent results in terms of three-wave mixing efficiencies in AlOx-based waveguides, this material has still considerable margins of amelioration for the most demanding photonics applications, and its fine understanding is a matter at the intersection of device physics and materials science.

3. THE OPO CAVITY

In view of the parametric oscillation, the choice of the cavity configuration has been made between the two practical optical resonators on which OPOs are mainly based, namely the singly resonant (SR) cavity and the doubly resonant (DR) one. In the first (resp. second) case, the cavity mirrors reflect only one (resp. both) of the signal/idler wavelengths. Since the pump threshold of the latter is typically one order of magnitude smaller than that of the former, we opted for a DR configuration, at the expense of a poorer spectral stability and tunability [1,34]. For a symmetric DR cavity with single pass of the pump, the steady-state pump power oscillation threshold P_{th} , which is minimum at degeneracy, reads [35]:

$$P_{th} = \frac{1}{\eta_{norm}} \left[\frac{\alpha_p/2}{1 - e^{-\alpha_p L/2}} \ln \left(R_{s,i} e^{-\alpha_{s,i} L} \right) \right]^2 \quad (1)$$

where η_{norm} is the waveguide normalized conversion efficiency, α_p is the pump loss, $\alpha_{s,i}$ is the signal/idler loss, L is the waveguide length, and $R_{s,i}$ is the modal reflectivity at signal/idler wavelength. We remind that for a phase-matched interaction in a lossy waveguide, η_{norm} is itself a function of L and α_j [34]. Plugging our experimental loss values of in Eq. 1, we find that for the pump threshold to be ≤ 100 mW, the mirrors modal reflectivity at degeneracy should be ≥ 98 % in a waveguide of optimal length $L \approx 2$ mm. Therefore, the nominal requirements of our mirrors were: 1) a broad high-reflectivity (HR) stopband centered about $\lambda=2.12$ μm with $R_{\text{max}}=99\%$; and 2) an anti-reflection (AR) window around $\lambda = 1.06$ μm with $R_{\text{min}} = 0.5$ %.

To meet these specifications, we opted for Bragg dielectric dichroic mirrors to be deposited onto waveguide facets. Their multilayer structure has been designed using the Essential MacLeod commercial software [36]. The widespread $\text{SiO}_2/\text{TiO}_2$ coating materials have been chosen for the bilayers of both mirrors, owing to their relatively high-index-contrast in the near infrared ($\Delta n \sim 0.8$) that enables to keep the thickness of the stack to a minimum. Six such bilayers turned out to be necessary to fulfill requirements.

The fabrication protocol that we have developed is based on Ion beam Assisted Deposition (IAD) that enables the coating at relatively low temperature, hence avoiding to anneal the sample, which could possibly alter the material quality. After oxidation, and prior to cleaving the sample facets, its surface is shielded from dielectric material overspray with a photoresist film (Shipley S1828 baked at 120°C for 5 min) that is eventually stripped.

A SEM picture of a waveguide facet after mirror deposition is shown in Fig. 3 (Left), where the mirror appears in the form of a dielectric “wall”. Besides the morphologic study of the fabricated cavities, we characterized them by measuring the mirrors reflectivity.

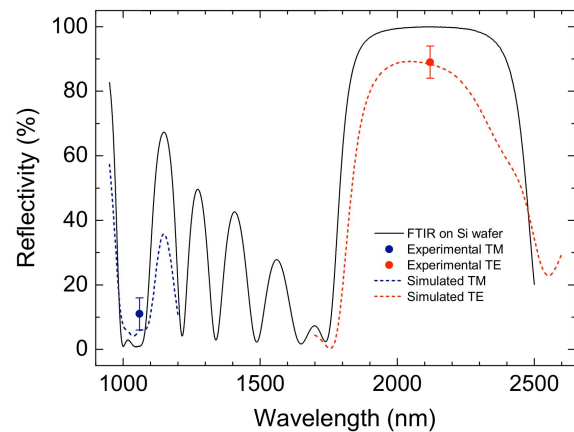
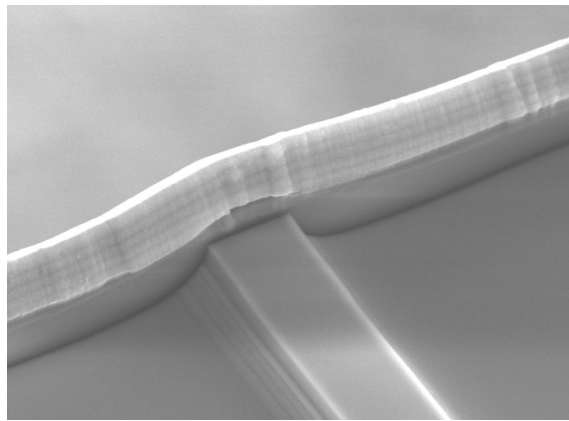


Figure 3. Left: Scanning-electron microscope view of one of the waveguide facets after mirror deposition. Right: Modal reflectivity of OPO monolithic mirrors. The measured values for TM_{00} pump at 1.064 μm and for TE_{00} signal and idler at 2.128 μm (dots) are in good agreement with numerical calculations (dashed lines). The picture is completed by the FTIR spectrum of a reference mirror (solid line) deposited on a Si planar substrate placed next to our sample during the fabrication of the integrated Bragg structure.

In order to validate the multilayer design, a silicon wafer placed in the deposition chamber close to our sample and coated during the same run, served as control sample to check the reflectivity spectrum of one mirror. The related experimental Fourier transform IR (FTIR) spectrum is shown in Fig. 3 (Right), along with modal reflectivities measured at $\lambda = 1.06$ μm and $\lambda = 2.12$ μm , respectively for the TM_{00} and TE_{00} modes. The former value has been inferred from a transmission measurement, resulting in $R_p = 11 \pm 5$ %. The latter has been inferred from the study of the Fabry-Perot fringes of a waveguide having one of its facets coated. A reflectivity $R_{s,i} = 90 \pm 5$ % has been estimated from the finesse of the Airy function fitting the data.

While the FTIR spectrum meets the theoretical requirements in terms of AR at λ_p and broad HR stop-band at $\lambda_{s,i}$ around degeneracy, the measured modal reflectivities differ significantly from the target values. Such discrepancy is attributed

to the 1D design procedure and the FTIR measurement, which only consider plane waves at normal incidence, while guided-modes also experience diffraction losses at each reflection. The experimental data are in better agreement with FDTD numerical calculations of the TM_{00} (resp. TE_{00}) mode reflectivity around $\lambda = 1.06 \mu\text{m}$ (resp. $2.12 \mu\text{m}$) accounting for this effect. Let us note that, even if the best agreement is obtained with accurate 3D-FDTD calculations, an acceptable alternative is obtained with the less-time consuming 2D-FDTD calculations (which only accounts for the vertical mode confinement).

4. EXPERIMENTAL RESULTS AND DISCUSSION

Both SPDC and OPO experiments have been performed with a TE polarized, CW Ti:Sapphire laser, tunable from 950 nm to 1100 nm with a linewidth around 30 GHz. A half-wave plate is used to obtain the TM polarized pump beam that is coupled into the sample with a $60\times$ microscope objective (0.85 NA) mounted on a piezoelectric positioning system. At the output, the pump beam is filtered out with a long-pass interferential filter and the IR beams are collected with a similar objective (a Glan-Taylor polarizer is used to verify the polarization selection rules). The latter are then focused onto an InGaAs photodiode, either directly or after passing through a monochromator. The photocurrent is measured with a low-noise transimpedance amplifier followed by a lock-in.

We started by measuring a parametric gain coefficient below threshold of $4.1 \text{ W}^{-1/2} \text{ cm}^{-1}$ at degeneracy, in agreement with our calculations [37]. The huge waveguide dispersion at pump wavelengths results in an extremely large tuning range for signal and idler ($>2800 \text{ nm}$ for a 70 nm variation in pump wavelength). Fig. 4 shows the SPDC tuning curve in the narrower spectral region of interest here.

Based on our experimental values of single-pass SPDC efficiency ($\eta_{\text{norm}} = 1500\% \text{ W}^{-1} \text{ cm}^{-2}$), reflectivity ($R_{s,i} = 90\%$) and losses ($\alpha_p \approx 3.0 \text{ cm}^{-1}$ and $\alpha_{s,i} \approx 1.0 \text{ cm}^{-1}$), Eq. 1 predicts a minimum for $L=2 \text{ mm}$, given by $P = 210 \text{ mW}$. Reaching this threshold has been a challenging task, mainly due to the unconventional mirror deposition onto the facets of our highly confining ridge waveguides. Despite this technological problem, some of our waveguide cavities have allowed us to observe a clear signature of OPO threshold behavior. This is shown in Fig. 5 (Left), where a distinct threshold is apparent for $P_{\text{th}} \approx 210 \text{ mW}$ (internal value), in full agreement with the above predictions. In Fig. 5 (Right) we also show the total SPDC power versus pump wavelength measured near degeneracy and below threshold, showing a good agreement with our simulations.

With the measured value of P_{th} , which corresponds to a mode intensity of $0.8 \times 10^7 \text{ W/cm}^2$, we can estimate two-photon absorption losses, obtaining $\alpha_{\text{TPA}} \approx 0.19 \text{ cm}^{-1}$, negligible with respect to the linear absorption at pump wavelength.

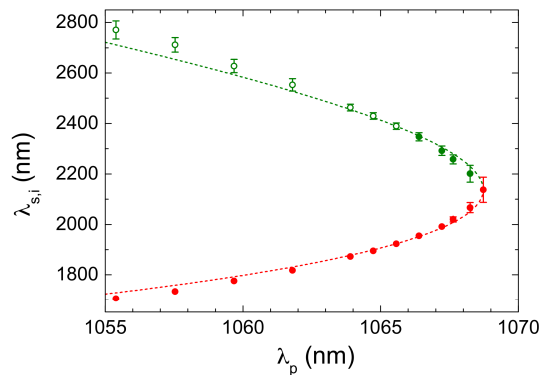


Figure 4. SPDC tuning: experimental data (dots) and best-fit curve. The measurements being limited to $\lambda \leq 2350 \text{ nm}$ due to detector cut-off, the idler data above this wavelength (circles) are inferred from energy conservation.

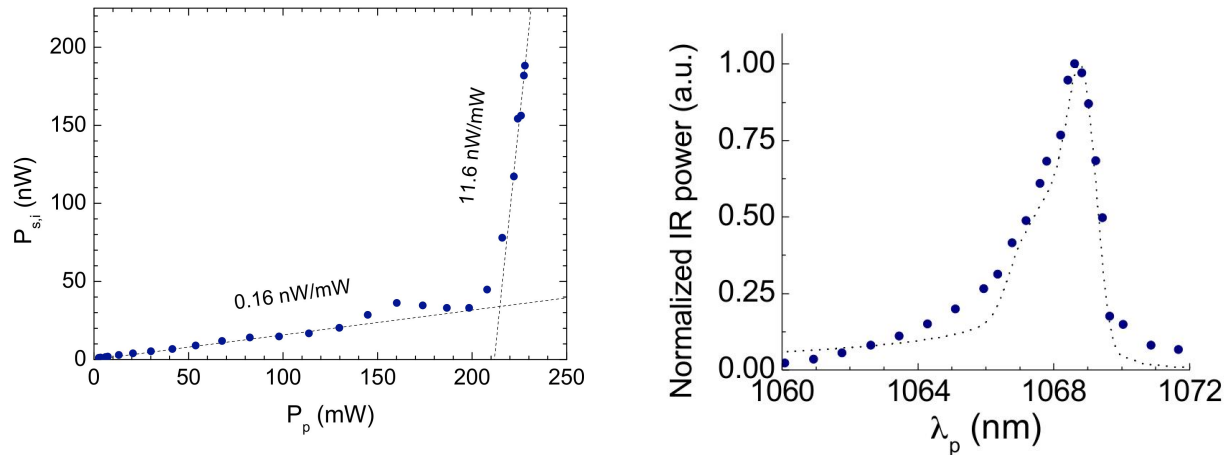


Figure 5. Left: OPO output power vs. pump power at degeneracy ($\lambda_p \approx 1068.5$ nm, $\lambda_{s,i} \approx 2137$ nm). The factor-60 increase of the differential efficiency beyond $P_p=210$ mW is a clear evidence of OPO threshold. Right: Total SPDC power vs. pump wavelength near degeneracy, as measured (dots) and calculated (dashed line).

The maximum pump power $P_p \approx 230$ mW is presently limited by an irreversible thermal damage of the mirrors that occurs after about thirty minutes of CW operation. This restricts the ratio P_p/P_{th} (i.e. the number of times the pump power exceeds the threshold) to 1.09, with of course an impact on the present maximum OPO power $P_{s,i} \approx 190$ nW.

5. CONCLUSION AND PERSPECTIVES

Beyond the present achievement of the OPO threshold, our future efforts will conveniently be devoted to increase P_p/P_{th} . To this end, a double-pass-pump scheme could be implemented, leading to a reduction of P_{th} by a factor between 2 and 4, depending on the relative dephasing of pump, signal, and idler modes at the back mirror of our DROPO. [38] Such scheme could also be adopted for a singly resonant OPO for which, despite a higher impact of TPA, we estimate a threshold $P_{th} \approx 0.8$ W: a reasonable price for its better stability and tunability performance.

A further optimization of our AlGaAs/AlOx OPO will demand reducing its near-IR linear propagation losses, which are caused by the oxidation of the Al-rich layers. The example of PPLN cavities is instructive because the fabrication of longer waveguides, possible thanks to their extremely low losses (< 0.1 cm⁻¹), enables a drastic reduction of the OPO threshold [6]. In this regard, many aspects of the lateral oxidation of AlGaAs layers are not clear yet, including the exact formation mechanisms and the fine chemical and structural properties of AlOx. Although oxidation is clearly responsible for the deterioration of the multilayer morphology, we have recently reported that the relatively low Rayleigh-like scattering losses due to AlOx/AlGaAs interface roughness only prevail at signal and idler wavelengths, whereas some volume effects must be considered to explain the higher losses at pump wavelengths, which constitute the bottleneck for our present results [22]. A systematic material optimization is currently under way and will hopefully push forward the performance of our AlOx waveguide cavity.

Finally, for future power scaling, we will explore the option of encapsulating the guiding ridge in e.g. benzocyclobutene (BCB), so that the mirrors can be deposited on wider facet areas, with an advantage in terms of uniformity and heat sink.

Besides improving the optically pumped OPO reported here, we also envisage to fabricate its electrically injected counterpart. A concrete design option would be to cascade the laser and OPO sections within one monolithic device, where we would selectively stop the lateral oxidation process before the complete hydrolyzation of the AlGaAs layers. We estimate that such VCSEL-like engineering of current and light confinement will lead the way to an electrically pumped OPO.

ACKNOWLEDGEMENTS

We thank X. Marcadet for MBE growth and the SEAM Labex of Sorbonne Paris Cité for financial support (DOLPHIN project).

REFERENCES

- [1] M. Ebrahimzadeh and M. H. Dunn, Handbook of Optics, Optical Society of America, 2nd Ed., Vol. IV (McGraw Hill, 2001).
- [2] Z. I. Alferov, V. M. Andreev, D. Z. Garbuzov, Y. V. Zhilyaev, E. P. Morozov, E. L. Portnoi, and V. G. Trofim, Sov. Phys. Semicond. 4, 1573 (1971).
- [3] J. A. Giordmaine and R. C. Miller, Phys. Rev. Lett. 14, 973 (1965).
- [4] W. Sohler, B. Hampel, R. Regener, R. Ricken, H. Suche, and R. Volk, IEEE J. Lightwave Technol. LT-4, 772 (1986).
- [5] M. L. Bortz, M. A. Arbore, and M. M. Fejer, Opt. Lett. 20, 49 (1995).
- [6] M. A. Arbore and M. M. Fejer, Opt. Lett. 22, 151 (1997).
- [7] A. L. Coldren, S. W. Corzine, and M. L. Mašanović, "Diode lasers and photonic integrated circuits" (Wiley, New York, 2012).
- [8] Focus issue on silicon photonics, Nature Photonics 4, August (2010).
- [9] A. S. Helmy, P. Abolghasem, J. S. Aitchison, B. J. Bijlani, J. Han, B. M. Holmes, D. C. Hutchings, U. Younis, and S. J. Wagner, Laser & Photon. Rev. 5, 272 (2011).
- [10] X. Yu, L. Scaccabarozzi, A. Lin, M. Fejer and J. Harris, J. Crystal Growth 301-302, 163 (2007).
- [11] S. Ducci, L. Lanco, V. Berger, A. De Rossi, V. Ortiz, and M. Calligaro, Appl. Phys. Lett. 84, 2974 (2004).
- [12] J. Han, P. Abolghasem, D. P. Kang, B. J. Bijlani, A. S. Helmy, Opt. Lett. 35, 2334 (2010).
- [13] A. Fiore, V. Berger, E. Rosencher, P. Bravetti, and J. Nagle, Nature 391, 463 (1998).
- [14] A. Grisard, E. Lallier, and B. Gérard, Opt. Mat. Expr. 2, 1020 (2012).
- [15] M. Oron, P. Blau, S. Pearl et M. Katz, Proc. SPIE 8240, 82400C (2012).
- [16] M. Born and E. Wolf, "Principles of Optics" (Pergamon, Oxford, 1980).
- [17] J. P. Van der Ziel, "Phase-matched harmonic generation in a laminar structure with wave propagation in the plane of the layers", Applied Physics Letters 26, 60 (1975).
- [18] Dallesasse J. M., Holonyak N., Sugg A. R., Richard T. A., and El-Zein N., Hydrolyzation oxidation of Al_xGa_{1-x}As-AlAs-GaAs quantum-well heterostructures and superlattices. Applied Physics Letters 1990; 57 (26) 2844.
- [19] Chen E. I., Holonyak Jr. N., and Maranowski S. A., Al_xGa_{1-x}As-GaAs metal-oxide semiconductor field effect transistors formed by lateral water vapor oxidation of AlAs. Applied Physics Letters 1995; 66 (20) 2688.
- [20] MacDougal M. H., Dapkus P. D., Pudikov V., Zhao H., Yang G. M., Ultralow threshold current vertical-cavity surface-emitting lasers with AlAs oxide-GaAs distributed Bragg reflectors. IEEE Photonics Technology Letters 1995; 7 (3) 229.
- [21] Huffaker D. L., Deppe D. G., Kumar K., and Rogers T. J., Native oxide defined ring contact for low threshold vertical cavity lasers. Applied Physics Letters 1994; 65 (1) 97.
- [22] M. Savanier, A. Andronico, A. Lemaître, C. Manquest, I. Favero, S. Ducci, and G. Leo, "Nearly-degenerate three-wave mixing at 1.55 μ m in oxidized AlGaAs waveguides," Opt. Exp. 19, 22582–22587 (2011).
- [23] A. Fiore, S. Janz, L. Delobel, P. van der Meer, P. Bravetti, V. Berger, E. Rosencher, and J. Nagle, "Second-harmonic generation at $\lambda=1.6\mu$ m in AlGaAs/Al₂O₃ waveguides using birefringence phase matching," Appl. Phys. Lett. 72, 2942–2944 (1998).
- [24] K. Choquette, K. Geib, C. Ashby, R. Twesten, O. Blum, H. Hou, D. Follstaedt, B. Hammons, D. Mathes, and R. Hull, "Advances in selective wet oxidation of AlGaAs alloys," IEEE J. Sel. Top. Quant. Electron. 3, 916–926 (1997).
- [25] G. Schreiber, D. Hofmann, W. Grundkoetter, Y. L. Lee, H. Suche, V. Quiring, R. Ricken, and W. Sohler, Wolfgang, "Nonlinear integrated optical frequency converters with periodically poled Ti:LiNbO₃ waveguides," Proc. SPIE 4277, 144–160 (2001).
- [26] E. Guillotel, C. Langlois, F. Ghiglieno, G. Leo, and C. Ricolleau, "TEM characterization of oxidized AlGaAs/AlAs nonlinear optical waveguides," J. Phys. D: Appl. Phys. 43, 385302 (2010).
- [27] A. De Rossi, V. Ortiz, M. Calligaro, L. Lanco, S. Ducci, V. Berger, and I. Sagnes, "Measuring propagation loss in a multimode semiconductor waveguide," J. Appl. Phys. 97, 073105 (2005).
- [28] J. A. Kash, B. Pezeshki, F. Agahi, and N. A. Bojarczuk, "Recombination in GaAs at the AlAs oxide-GaAs interface," Appl. Phys. Lett. 67, 2022–2024 (1995).
- [29] J. F. Chen, R. S. Hsiao, W. K. Hung, J. S. Wang, J. Y. Chi, H. C. Yu, and Y. K. Su, "Evolution of conduction and interface states of laterally wet-oxidized AlGaAs with oxidation time," J. Appl. Phys. 99, 023711 (2006).
- [30] A. G. Baca, and C. I. H. Ashby, Fabrication of GaAs Devices (Institution of Electrical Engineers, 2005).

- [31] S. Shi, E. Hu, J.-P. Zhang, Y.-L. Chang, P. Parikh, and U. Mishra, "Photoluminescence study of hydrogenated aluminum oxide-semiconductor interface," *Appl. Phys. Lett.* 70, 1293–1295 (1997).
- [32] F. Chouchane, G. Almuneau, O. Gauthier-Lafaye, A. Monmayrant, A. Arnoult, G. Lacoste, and C. Fontaine, "Observation of overstrain in the coalescence zone of AlAs/AlO_x oxidation fronts," *Appl. Phys. Lett.* 98, 261921 (2011).
- [33] S.-C. Lee, and W.-I Lee, "Ga_{0.5}In_{0.5}P barrier layer for wet oxidation of AlAs," *Jpn. J. Appl. Phys.* 39, 2583-2584 (2000).
- [34] R. Sutherland, *Handbook of nonlinear optics* (Marcel Dekker, 2003).
- [35] G. Bava, I. Montrosset, W. Sohler, and H. Suche, "Numerical modeling of Ti:LiNbO₃ integrated optical parametric oscillators," *IEEE J. Quantum Electron.* 23, 42–51 (1987).
- [36] H. Macleod, *Thin-film optical filters* (CRC Press, 2010).
- [37] E. Guillotel, M. Ravaro, F. Ghiglieno, C. Langlois, C. Ricolleau, S. Ducci, I. Favero, and G. Leo, *Appl. Phys. Lett.* 94, 171110 (2009).
- [38] J. E. Bjorkholm, A. Ashkin, and R. G. Smith, "Improvement of optical parametric oscillators by nonresonant pump reflection, *IEEE J. Quantum Electron.* QE-6, 797-799 (1970).